60 años cuidando nuestros suelos

CIENCIA DEL SUELO

ON-THE-GO SENSOR WITH EMBEDDED LOAD CELLS FOR MEASURING SOIL MECHANICAL RESISTANCE

FEDERICO RAFAEL MASCH[1]*; ROGELIO LORENZO HECKER[1-3]; GUSTAVO MARCELO FLORES[1]; PABLO REMIREZ[1]; ROMINA FERNANDEZ[2]

Recibido: 09/08/2019
Recibido con revisiones: 26/09/2019
Aceptado: 22/10/2019

ABSTRACT

Soil compaction is an important degradation phenomenon that can affect root growth, and consequently crop yield. Therefore it becomes relevant to have soil compaction data for future improvements on precision agriculture management. A traditional on-the-field data related to soil compaction is cone index obtained using a penetrometer; however, this methodology is time consuming for a high density data. Therefore, on-the-go sensors have been developed to continually estimate the variable of interest. This work proposes an on-the-go sensor to estimate the soil horizontal resistance at different depths. The main design concept is based on embedded load cells at three different depths, resulting in a robust sensor with high sensitivity. The prototype was first tested and calibrated in laboratory, and then, it was tested in the field. The calculated horizontal resistance index (HRI) at the three depths was correlated with the cone index (CI) using a cone penetrometer, showing that this sensor can replace the penetrometer data, allowing the possibility of taking continuous data on the field.

Keywords: soil compaction; on-the-go sensor; soil mechanical resistance.

SENSOR CON CELDAS DE CARGA EMBEBIDAS PARA LA MEDICIÓN DE LA RESISTENCIA MECÁNICA DEL SUELO

RESUMEN

La compactación de los suelos agrícolas es un fenómeno que afecta el normal desarrollo de las raíces de los cultivos y consecuentemente su posterior rendimiento. Por lo tanto, disponer de la información del estado de compactación del suelo será relevante en un futuro en lo que respecta a la agricultura de precisión. La información usual recolectada en campo relacionada con la compactación del suelo es el índice de cono (CI), obtenido mediante el uso del penetrómetro. Sin embargo, la obtención de dicha información con una alta resolución espacial a partir del penetrómetro resulta ineficiente y altamente costosa. Atendiendo a esta dificultad, se han desarrollado sensores on-the-go, cuya principal característica es su capacidad de registrar de manera continua la resistencia mecánica del suelo, con una alta resolución espacial tanto en el plano horizontal como en el vertical. Dicha característica reduce de manera significativa los tiempos y los costos de adquisición de la información de la resistencia mecánica del suelo, por la cual a partir de la misma se estima el estado de compactación del suelo. En este trabajo se presenta un sensor para medir de forma continua la resistencia mecánica del suelo en tres profundidades diferentes del suelo. En este dispositivo se utilizan celdas de cargas embebidas en el propio seno de dicho sensor promoviendo así un desempeño robusto y con una alta sensibilidad. El prototipo de este sensor fue en primera instancia evaluado y calibrado en laboratorio, para luego finalmente evaluar su desempeño en pruebas a campo. La resistencia mecánica horizontal del suelo en los tres intervalos de profundidad relevados por dicho sensor ha sido correlacionada con el índice de cono (CI) obtenido mediante un penetrómetro, mostrando que resulta factible la utilización de la información relevada por este sensor en la estimación del estado de compactación del suelo.

Palabras claves: compactación del suelo; sensor sobre la marcha; resistencia mecánica del suelo.

1 Facultad de Ingeniería Universidad Nacional de La Pampa. Argentina

2 Instituto Nacional de Tenologías Agropecuarias. Anguil. Argentina

3 CONICET. Argentina

* Autor de contacto: **maschfederico@gmail.com**

INTRODUCTION

Precision agriculture demands identification and determination of soil factors that affect crop yield. Of the various factors involved, soil compaction is an important degradation phenomenon producing changes in soil structure, reducing macroporosity and increasing bulk density. These changes reduce the soil capacity of gas exchange and decrease water infiltration rate, affecting root growth and crop yield.

The methodologies usually used for measuring soil compaction are bulk density determination of soil samples and mechanical strength measurements using penetrometers. However, these techniques are time demanding; therefore, they are not suitable for high density data of soil compaction in large fields (Adamchuk *et al.*, 2004).

In recent years, this concern has promoted the development of on-the-go sensors that provide a high density data at relatively low cost and short times (Hemmat & Adamchuk, 2008; Rahimi-Ajdadi *et al.*, 2017). Regarding the on-the-go sensors to estimate soil compaction, these are mainly based on mechanical interaction between a moving blade and the soil. These sensors can be arranged into two groups according to their spatial resolution. The first group measures the total force of the soil-blade interaction using a single load cell, giving only the horizontal variability (Godwin, 1975; Glancey *et al.*, 1989; Mouazen & Ramon, 2006; Sun *et al.*, 2011) as the blade moves in the field. The second group of sensors allows to measure or estimate also the vertical variability of soil resistance in the soil profile. To achieve this latter goal, Adamchuk *et al* (2001) installed strain gages at the back of a blade to measure the generated mechanical strain and then to estimate force values at discrete positions on the blade front. Alternatively, the authors propose a second design concept in order to estimate the parameters of a continuous force profile in the blade front, based also on strain gauges measurements. Other researchers directly measure the soil strength at different depths by installing load cells at discrete vertical positions in the blade front. Particularly, Andrade-Sanchez *et al,* (2007) installed eight load cells in the blade front to measure the mechanical stresses generated in prismatic tips with 5 cm high. Alternatively, Chung *et al.* (2006) has used commercial cylindrical load cells with prismatic tips, vertically spaced at 10 cm. Similar developments with individual installed load cells can be found in (Hemmat *et al.*, 2009; Abbaspour-Gilandeh & Rahimi-Ajdadi, 2012; Hemmat *et al.*, 2013; Hemmat *et al.*,2014).

Embedded strain gauges presents a more robust design than individual assembled load cell, because the latter involves assembled and some times moving parts, which could be a problem for a blade moving into the soil. However, the efficiency of the blades with strain gauges installed in the blade back, depends on the mathematical model to estimate the front stresses with a predefined profile. Therefore, the goal of this work is to present a robust design of a blade with embedded load cells and with no moving parts.

Based on the reviewed sensors, the objective of this work is to obtain a sensor to directly measure the soil mechanical resistance at different soil depths with low crosstalk between these measurements.

DESIGN

Conceptual design

The design was based on machining of three embedded load cells in the blade front, as shown in **Figure 1**. In this way, each load cell estimates the force over a discrete area in the blade front through local deformation measurements, given

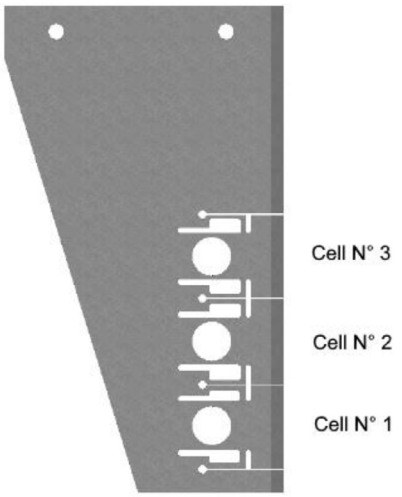

Figure 1. Embedded load cell array in the blade front.

Figura 1. Celdas de cargas mecanizadas en el frente de la cuchilla.

by strain gauges at two specific zones on an internal cylindrical surface. **Figure 2** shows a numerical simulated load cell for an applied external pressure, where the zones with high strains are clearly observed in the lower and upper part of this internal cylindrical surface.

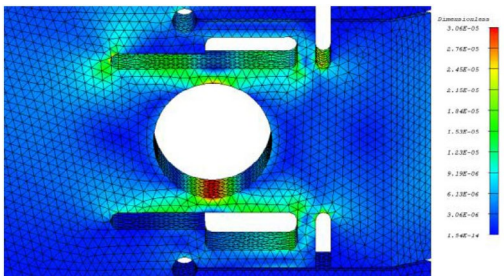

Figure 2. Example of compression strain values for an applied uniform pressure.

Figura 2. Deformación de la celda de carga ante una presión uniforme en el frente de la celda mediante simulaciones por elemento finito.

The thickness e_1 in **Figure 3** is the main design variable that fixes the relation between strain measures and applied forces on each load cell. The load cell sensitivity increases as e_1 decreases, but this tendency negatively affects the overall lateral rigidity of each load cell. Therefore, to maintain the integrity to lateral forces, an L-shape linkage was introduced, as can be seen as shaded areas in **Figure 3**, which increases lateral rigidity with low effect on the load cell sensitivity. This linkage is characterized by L_2, L_1 and the thickness e_2.

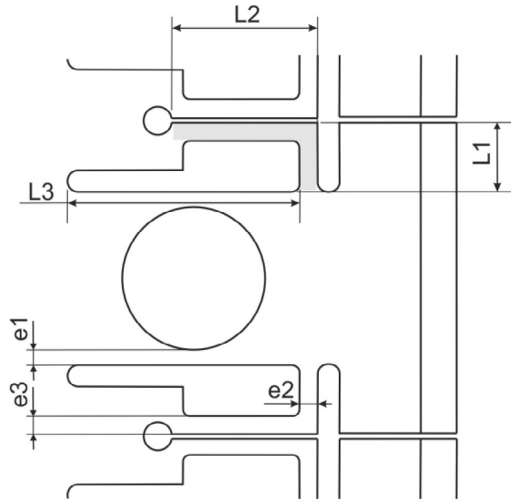

Figure 3. Internal geometry of a cell and its characteristic dimensions L_1, L_2, L_3, e_1, e_2 and e_3.

Figura 3. Geometría interna de la celda de carga y sus dimensiones características L_1, L_2, L_3, e_1, e_2 y e_3.

On the other hand, the blade is like a cantilever beam fixed at its top; therefore, an applied force on a lower cell generates strains and then parasitic measurements on the upper cells. To reduce this effect, called crosstalk between cells, a series of horizontal cuts are machined between cells, characterized by the length L_3, as can be seen in **Figure 3**.

In this way, it is possible to design a blade with embedded load cells achieving desired sensitivity to applied front forces, high lateral rigidity, and reduced crosstalk between cells, as it is shown next.

Design specifications

The selected length of the blade front is 240 mm, where each load cell covers 80 mm. The thickness e_1 of each load cell was selected in order to have higher sensitivity at the cells closer to the ground surface. This is because it was reported that for a moving blade, the pressure to break the soil increases with the depth (Adamchuk *et al.*, 2008). As a reference, the interaction pressure assumed close to surface is 0.5 MPa and a maximum of 4 MPa at the deepest cell.

Therefore, a desired sensitivity S, given by the ratio between the generated strain at the high deformation zones and the applied external pressure, was specified for each cell. The selected values are $S_1 = 50\ 10^{-6}$ MPa^{-1} for cell N°1, the deepest one, $S_2 = 90\ 10^{-6}$ MPa^{-1} for cell N°2 located in the middle, and $S_3 = 120\ 10^{-6}$ MPa^{-1} for cell N°3 located near surface. In this way, when cell N°1 is subject to 4 MPa it will be at 50% from yielding, which means a design safe factor of two considering a blade made of plane steel. On the other hand, it is desired to have at least 0,1 MPa of resolution on cell N°3, which in this case corresponds to a strain of $12\ 10^{-6}$. This last value is perfectly measured by the strain gauge configuration and the instruments presented in next section.

To achieve the desired sensitivities values for each cell, the initial values of thickness e_1 were first calculated using a mathematical model for circular rings reported in Karabay (2007). After that, they were adjusted iteratively using FEM

(Finite Element Model) simulations by applying a distributed force on each cell front and by measuring the the strain values in the high deformation zones. The other load cell geometrical parameters, shown in **Figure 3** were also adjusted with FEM simulations in order to guarantee high lateral rigidity, reduced crosstalk between cells, and at the same time, not affecting considerably the cells sensitivity. Finally, the angle of attack of the blade front was set to α=60° and it was selected to minimize the draft according to Chung *et al.* (2006).

IMPLEMENTATION AND CALIBRATION

Instrumentation

The blade was built from a laminated steel SAE 1010 of 25 mm of thickness, where milling and cutting process were used to give the overall blade shape and to machine each load cell. Particularly, the internal cylindrical surface of the machined load cells was polished to generate a smooth surface to glue the strain gauges.

A full bridge configuration with four strain gauges, model SG-3/350-LY11 from Omega, were used in each cell. As it is observed in **Figure 4**, the strain gauges SG1 and SG2 were installed in the areas of maximum strain, as it was studied by FEM simulation in **Figure 2**. Furthermore, these strain gauges were oriented in the direction of maximum compression deformation. The other two strain gauges, SG3 and SG4 in **Figure 4**, were used for temperature compensation; therefore, they were installed within the internal cylindrical surface where the mechanical deformations are null or minimum, with a 90° orientation with respect to SG1 and SG2.

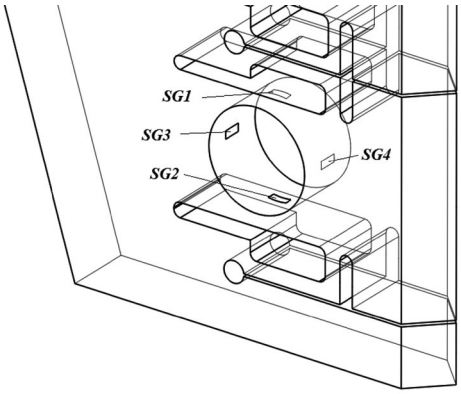

Figure 4. Strain gauges locations in the cell.

Figura 4. Localización de las galgas extensiométricas sobre la celda de carga.

The signal from each bridge was first conditioned by ICP-DAS SG-3016 and after that, recorded by a portable data acquisition system, Ueisim 600-1G, with an analog to digital board with 16 bits of resolution. The gauge factor for each strain gauge is two, the excitation voltage for each bridge was set to 5 V, and the signal conditioning system has a gain of 1000x. This configuration gives the following sensitivities values, now from the applied pressure to the output voltage, S_1=250 mV MPa^{-1}, S_2=450 mV MPa^{-1} y S_3=600 mV MPa^{-1}

Laboratory test and calibration

Figure 5 shows the response of each cell, characterized by its conditioned signal output in mV, versus HRI. As can be seen, each cell fits a linear response with a high correlation factor. The slope of each response is the measured sensitivity for each cell, with S_1=260 mV MPa^{-1} for cell N°1, 450 mV MPa^{-1} for cell N°2, and S_3=600 mV MPa^{-1} for cell N°3, which are in close agreement with the designed values presented in the previous section.

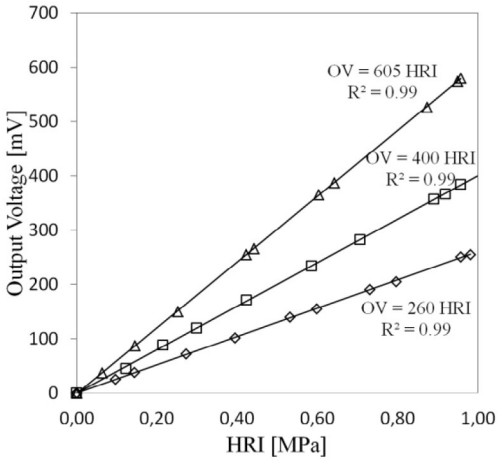

Figure 5. Output voltage response of each cell subjected to individually applied loads. Cell N°1 (diamond), cell N°2 (square), and cell N°3 (triangle).

Figura 5. Tensión de salida de cada unas de las celdas cuando se aplica individualemente una carga sobre las mismas. Celda N°1 (diamante), celda N°2 (cuadrado), and celda N°3 (triángulo).

A second set of test consisted in applying forces to an individual cell and analyze the response of the other cells. **Figure 6** shows an example where the external pressure is applied only on cell N°1, and it can be observed that cell N°2 and cell N°3 are presenting a low response. This is the most critical condition to evaluate crosstalk, because cell N°1 is the further cell from the blade fixing area; therefore, any applied force on this cell affects the reading of all the other cells. This low crosstalk is a consequence of the cell design explained in the conceptual design section. Finally, all the laboratory measured data is used to formulate the following calibration equation used to estimate the applied pressure on each cell, Pj in MPa, from the output voltage of each conditioned cell, Vj mV:

$$P_1 = 3.84\ 10^{-3}V_1 - 3.51\ 10^{-5}V_2 - 2.83\ 10^{-5}V_3 \quad (1)$$

$$P_2 = -1.05\ 10^{-4}V_1 - 2.49\ 10^{-3}V_2 - 6.06\ 10^{-6}V_3 \quad (2)$$

$$P_3 = -1.78\ 10^{-4}V_1 - 6.29\ 10^{-5}V_2 + 1.65\ 10^{-3}V_3 \quad (3)$$

The elements in the diagonal are the direct response of each cell, which are directly the inverse of the measured sensitivities. On the other hand, the out of diagonal elements are the values to compensate the remanent crosstalk between the cells. It can be observed that the out of diagonal elements are at least one order of magnitude lower than the diagonal ones, which is a consequence of the mechanical decoupling obtained from the design process. Now, a complete decoupling can be obtained using Eq.(1), Eq.(2) and Eq.(3)

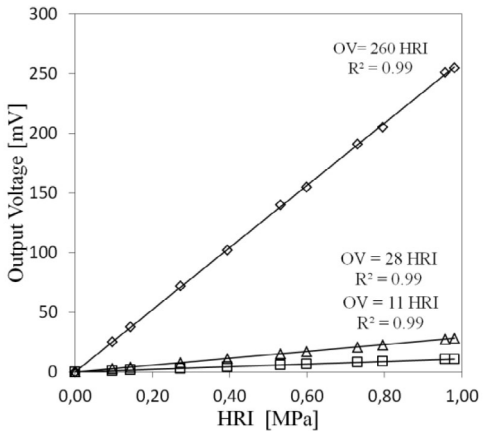

Figure 6. Output voltage response of cell N°2 (square) and cell N°3 (triangle) when a load is applied to cell N°1 (diamond).

Figura 6. Tensión de salida de la celda N°2 (cuadrado) y celda N°3(triángulo) ante una carga aplicada sobre la celda N°1(diamante).

FIELD EXPERIMENTS

The study site was a field next to Embajador Martini, La Pampa, Argentina (35° 25' 40"S, 64°16'10" W, 178 m above sea level). The weatherclimate can be characterized as mild with a mean annual precipitation of 700 mm and a mean temperature of 16°C. The soil under study corresponds to the Mollisol taxonomic order with a genetic evolution with little differentiation of horizons, a texture of loam to a texture of sandy loam, with a calcareous horizont of 800 mm.

The field experiments have been carried out in winter. The field was under fallow in the previous year. The soil samples were analyzed in the laboratory yielding the following results: 9.8% of clay, 21.5% of silt, 68.7% of sand, 1.0**%** of organic matter, 4.0 ppm of phosphorus, and 17% of gravimetric water content.

The blade was installed in a subsoiler frame, as can be seen in **Figure 7** and the working depth was set to 240 mm, in this way allowing the interaction of the three load cells with the soil profile. This figure also shows that the subsoilers that can interfere with the soil area affected by the sensor were removed before the experiments. The mean working velocity was of 1.1 ms^{-1} in straight paths. On the other hand, penetration resistance measurements were recorded with 50 mm increments over 250 mm of depth, using a manual penetrometer (O'Sullivan *et al.*, 1987). The data from every straight path from the blade was divided into segments equal to the number of penetrometer measurements over the same path. After that, the average value of soil horizontal resistance index (HRI) of every load cell over a given segment was correlated with the corresponding value of conex index (CI), obtained with the penetrometer. Spe-

Figure 7. Developed sensor installed on subsoiler.

Figura 7. El sensor instalado sobre un subsolador.

cifically, the CI values at a depth of 50 mm are related to the values of HRI measured by cell N°3 (0-80 mm), the mean CI values at depths of 100 mm and 150 mm were related to measurements of cell N°2 (80-160 mm), and the mean CI values at depths of 200 mm and 250 mm to measurements of cell N°1 (160-240 mm).

PRELIMINARY RESULTS AND DISCUSSION

The relations between HRI and CI are shown in **Figure 8** for cell N°3 at a depth of 0-80 mm, **Figure 9** for cell N°2 at a depth of 80-160 mm, and **Figure 10** for cell N°1 at a depth of 160-240 mm, where in each graph the data was fitted with straight lines. As can be seen, there is a better data correlation for the deeper cells. The correlation coefficients are equal to 0.42, 0.68, and 0.81 for the interval depths of 0-80 mm, 80-160 mm, and 160-240 mm, respectively.

The lower correlation between HRI and CI for cell N°3 can be attributed to the change in the soil type of fracture closer to the soil surface. The-

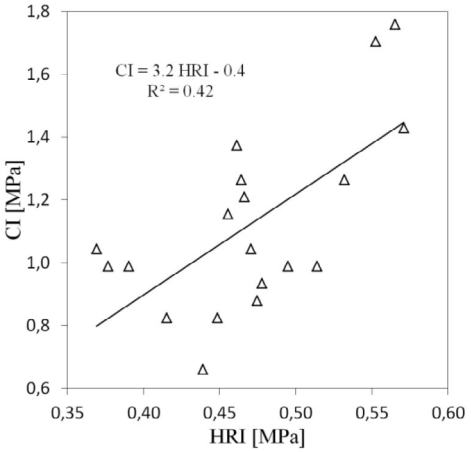

Figure 8. Correlation between the soil horizontal resistance index (HRI) and cone index (CI) for interval depth Cell N°3 (0-80 mm).

Figura 8. Correlación entre el índice de resistencia mecánica horizontal del suelo (HRI) y el índice de cono (CI) para el intervalo de profundidad correspondiente a la celda N°3 (0-80 mm).

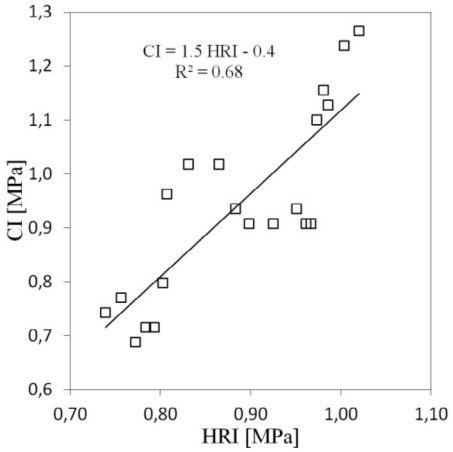

Figure 9. Correlation between the soil horizontal resistance index (HRI) and cone index (CI) for interval depth Cell N°2 (80-160 mm).

Figura 9. Correlación entre el índice de resistencia mecánica horizontal del suelo (HRI) y el índice de cono (CI) para el intervalo de profundidad correspondiente a la celda N°2 (80-160 mm).

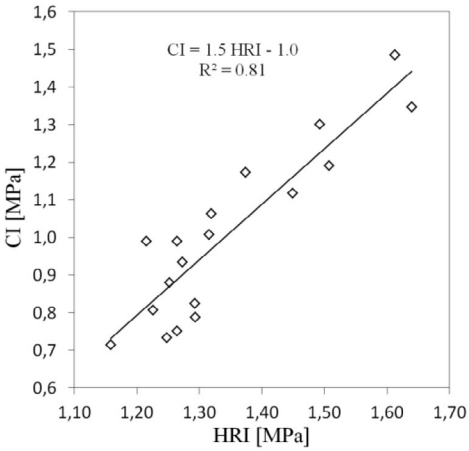

Figure 10. Correlation between the soil horizontal resistance index (HRI) and cone index (CI) for interval depth Cell N°1 (160-240 mm).

Figura 10. Correlación entre el índice de resistencia mecánica horizontal del suelo (HRI) y el índice de cono (CI) para el intervalo de profundidad correspondiente a la celda N°1 (160-240 mm).

re is a critical depth over which the soil tends to move upwards. By visual inspection in the field, this critical depth was estimated in 100 mm, similar to values reported by Hemmat *et al.*, (2012). Up to this depth, the soil has a fracture type of failure and undergoes frictional and adhesive forces with high variability. As a consequence, a higher variability or lower correlation factor can be observer in the upper load cell.

Below the critical depth, the soil fails with a bearing-capacity type, dominated by a lateral soil displacement, resulting in a resistance increase with the working depth showing lower data variability. At the same time, the soil failure mode using a vertical penetrometer is also a bearing-capacity type, (Chung & Sudduth, 2006). This characteristic also explains the increment of the correlation between HRI and CI for depths below the critical depth, similar results was reported by (Hemmat *et al.*, 2009, Hemmat *et al.*, 2013; Hemmat *et al.*, 2014).

CONCLUSIONS

A blade sensor with embedded load cells to measure soil horizontal resistance at different depth intervals was developed and preliminary tested in the field. The concept of directly machined and instrumented load cells in the blade front allows a robust design with adjusted sensitivity, high lateral rigidity and low crosstalk between cells.

First, in laboratory tests, the sensor shows a perfect linear response, high sensitivity to detect low values, and the expected low crosstalk. Second, in the field experiments it shows a good correlation between the blade HRI and the penetrometer CI for the cells below the critical depth, these are cell N°2 and particularly cell N°1. Therefore, the developed sensor has potential to map the mechanical resistance of soil profile with a total depth of 240 mm.

ACKNOWLEDGEMENT

This work is sponsored by an agreement between Facultad de Ingeniería UNLPam and INTA, Argentina.

BIBLIOGRAPHY

Abbaspour-Gilandeh, Y. & Rahimi-Ajdadi, F. (2012) 'A field comparison of two prototype sensors for horizontally on-the-go soil mechanical resistance measurement', *Measurement*. Elsevier, 45(7), pp. 1906–1912.

Adamchuk, V. I. *et al.* (2004) 'On-the-go soil sensors for precision agriculture', *Computers and Electronics in Agriculture*. doi: 10.1016/j.compag.2004.03.002.

Adamchuk, V. I. *et al.* (2008) 'On-the-go mapping of soil mechanical resistance using a linear depth effect model', *Transactions of the ASABE*. American Society of Agricultural and Biological Engineers, 51(6), pp. 1885–1894.

Adamchuk, V. I., Morgan, M. T. & Sumali, H. (2001) 'Application of a strain gauge array to estimate soil mechanical impedance on-the-go.', *Transactions of the ASAE*, 44(6), pp. 1377–1383.

Andrade-Sanchez, P., Upadhyaya, S. D. & M. Jenkins, B. (2007) 'Development, Construction, and Field Evaluation of a Soil Compaction Profile Sensor', *Transactions of the ASABE*, 50, pp. 719–725. doi: 10.13031/2013.23126.

Chung, S. O. & Sudduth, K. A. (2006) 'Soil failure models for vertically operating and horizontally operanting strength sensors', Trans. ASABE, 49(4), pp. 851–863.

Chung, S. O., Sudduth, K. & Hummel, J. W. (2006) 'Design and validation of an on-the-go soil strength profile sensor', *Transactions of the ASABE*, 49, pp. 5–14. doi: 10.13031/2013.20229.

Glancey, J. L. *et al.* (1989) 'An instrumented chisel for the study of soil-tillage dynamics', *Soil and Tillage Research*. Elsevier, 14(1), pp. 1–24.

Godwin, R. J. (1975) 'An extended octagonal ring transducer for use in tillage studies', *Journal of Agricultural Engineering Research*. Academic Press, 20(4), pp. 347–352. doi: 10.1016/0021-8634(75)90071-2.

Hemmat, A. *et al.* (2009) 'Influence of failure mode induced by a horizontally operated single-tip penetrometer on measured soil resistance', *Soil and Tillage Research*. Elsevier, 105(1), pp. 49–54.

Hemmat, A. *et al.* (2013) 'Development and field testing of an integrated sensor for on-the-go measurement of soil mechanical resistance', *Sensors and Actuators A: Physical. Elsevier*, 198, pp. 61–68.

Hemmat, A. and Adamchuk, V. I. (2008) 'Sensor systems for measuring soil compaction: Review and analysis', *Computers and Electronics in Agriculture*. Elsevier, 63(2), pp. 89–103. doi: 10.1016/J.COMPAG.2008.03.001.

Hemmat, A., Khorsandi, A. & Shafaie, V. (2012) 'Soil failure mode in front of a multiple-tip horizontally operated penetrometer', *Turkish Journal of Agriculture and Forestry*. The Scientific and Technological Research Council of Turkey, 36(4), pp. 476–485.

Hemmat, A., Rahnama, T. & Vahabi, Z. (2014) 'A horizontal multiple-tip penetrometer for on-the-go soil mechanical resistance and acoustic failure mode detection', *Soil and Tillage Research*. Elsevier, 138, pp. 17–25.

Karabay, S. (2007) 'Design criteria for electro-mechanical transducers and arrangement for measurement of strains due to metal cutting forces acting on dynamometers', *Materials & Design*. Elsevier, 28(2007), pp. 206–496.

Mouazen, A. M. & Ramon, H. (2006) 'Development of on-line measurement system of bulk density based on on-line measured draught, depth and soil moisture content', *Soil and Tillage Research*. Elsevier, 86(2), pp. 218–229.

O'Sullivan, M. F., Dickson, J. W. & Campbell, D. J. (1987) 'Interpretation and presentation of cone resistance data in tillage and traffic studies', *Journal of Soil Science*. Wiley Online Library, 38(1), pp. 137–148.

Rahimi-Ajdadi, Fatemeh & Abbaspour-Gilandeh, Y. (2017) 'A review on the soil compaction measurement systems', in *Conference on Organic vs. Conventional Agriculture*.

Sun, Y. *et al.* (2011) 'Map-based investigation of soil physical conditions and crop yield using diverse sensor techniques', *Soil and Tillage Research*. Elsevier, 112(2), pp. 149–158.